

Search for a light Higgs resonance in radiative decays of the $\Upsilon(1S)$ with a charm tag

J. P. Lees,¹ V. Poireau,¹ V. Tisserand,¹ E. Grauges,² A. Palano^{ab,3} G. Eigen,⁴ B. Stugu,⁴ D. N. Brown,⁵ L. T. Kerth,⁵ Yu. G. Kolomensky,⁵ M. J. Lee,⁵ G. Lynch,⁵ H. Koch,⁶ T. Schroeder,⁶ C. Hearty,⁷ T. S. Mattison,⁷ J. A. McKenna,⁷ R. Y. So,⁷ A. Khan,⁸ V. E. Blinov^{abc,9} A. R. Buzykaev^{a,9} V. P. Druzhinin^{ab,9} V. B. Golubev^{ab,9} E. A. Kravchenko^{ab,9} A. P. Onuchin^{abc,9} S. I. Serednyakov^{ab,9} Yu. I. Skovpen^{ab,9} E. P. Solodov^{ab,9} K. Yu. Todyshev^{ab,9} A. J. Lankford,¹⁰ B. Dey,¹¹ J. W. Gary,¹¹ O. Long,¹¹ M. Franco Sevilla,¹² T. M. Hong,¹² D. Kovalskyi,¹² J. D. Richman,¹² C. A. West,¹² A. M. Eisner,¹³ W. S. Lockman,¹³ W. Panduro Vazquez,¹³ B. A. Schumm,¹³ A. Seiden,¹³ D. S. Chao,¹⁴ C. H. Cheng,¹⁴ B. Echenard,¹⁴ K. T. Flood,¹⁴ D. G. Hitlin,¹⁴ T. S. Miyashita,¹⁴ P. Ongmongkolkul,¹⁴ F. C. Porter,¹⁴ M. Röhrken,¹⁴ R. Andreassen,¹⁵ Z. Huard,¹⁵ B. T. Meadows,¹⁵ B. G. Pushpawela,¹⁵ M. D. Sokoloff,¹⁵ L. Sun,¹⁵ P. C. Bloom,¹⁶ W. T. Ford,¹⁶ A. Gaz,¹⁶ J. G. Smith,¹⁶ S. R. Wagner,¹⁶ R. Ayad,^{17,*} W. H. Toki,¹⁷ B. Spaan,¹⁸ D. Bernard,¹⁹ M. Verderi,¹⁹ S. Playfer,²⁰ D. Bettoni^{a,21} C. Bozzi^{a,21} R. Calabrese^{ab,21} G. Cibinetto^{ab,21} E. Fioravanti^{ab,21} I. Garzia^{ab,21} E. Luppi^{ab,21} L. Piemontese^{a,21} V. Santoro^{a,21} A. Calcaterra,²² R. de Sangro,²² G. Finocchiaro,²² S. Martellotti,²² P. Patteri,²² I. M. Peruzzi,^{22,†} M. Piccolo,²² M. Rama,²² A. Zallo,²² R. Contri^{ab,23} M. R. Monge^{ab,23} S. Passaggio^{a,23} C. Patrignani^{ab,23} B. Bhuyan,²⁴ V. Prasad,²⁴ A. Adametz,²⁵ U. Uwer,²⁵ H. M. Lacker,²⁶ U. Mallik,²⁷ C. Chen,²⁸ J. Cochran,²⁸ S. Prell,²⁸ H. Ahmed,²⁹ A. V. Gritsan,³⁰ N. Arnaud,³¹ M. Davier,³¹ D. Derkach,³¹ G. Grosdidier,³¹ F. Le Diberder,³¹ A. M. Lutz,³¹ B. Malaescu,^{31,‡} P. Roudeau,³¹ A. Stocchi,³¹ G. Wormser,³¹ D. J. Lange,³² D. M. Wright,³² J. P. Coleman,³³ J. R. Fry,³³ E. Gabathuler,³³ D. E. Hutchcroft,³³ D. J. Payne,³³ C. Touramanis,³³ A. J. Bevan,³⁴ F. Di Lodovico,³⁴ R. Sacco,³⁴ G. Cowan,³⁵ D. N. Brown,³⁶ C. L. Davis,³⁶ A. G. Denig,³⁷ M. Fritsch,³⁷ W. Gradl,³⁷ K. Griessinger,³⁷ A. Hafner,³⁷ K. R. Schubert,³⁷ R. J. Barlow,^{38,§} G. D. Lafferty,³⁸ R. Cenci,³⁹ B. Hamilton,³⁹ A. Jawahery,³⁹ D. A. Roberts,³⁹ R. Cowan,⁴⁰ R. Cheaib,⁴¹ P. M. Patel,^{41,¶} S. H. Robertson,⁴¹ N. Neri^{a,42} F. Palombo^{ab,42} L. Cremaldi,⁴³ R. Godang,^{43,**} D. J. Summers,⁴³ M. Simard,⁴⁴ P. Taras,⁴⁴ G. De Nardo^{ab,45} G. Onorato^{ab,45} C. Sciacca^{ab,45} G. Raven,⁴⁶ C. P. Jessop,⁴⁷ J. M. LoSecco,⁴⁷ K. Honscheid,⁴⁸ R. Kass,⁴⁸ M. Margoni^{ab,49} M. Morandin^{a,49} M. Posocco^{a,49} M. Rotondo^{a,49} G. Simi^{ab,49} F. Simonetto^{ab,49} R. Stroili^{ab,49} S. Akar,⁵⁰ E. Ben-Haim,⁵⁰ M. Bomben,⁵⁰ G. R. Bonneaud,⁵⁰ H. Briand,⁵⁰ G. Calderini,⁵⁰ J. Chauveau,⁵⁰ Ph. Leruste,⁵⁰ G. Marchiori,⁵⁰ J. Ocariz,⁵⁰ M. Biasini^{ab,51} E. Manoni^{a,51} A. Rossi^{a,51} C. Angelini^{ab,52} G. Batignani^{ab,52} S. Bettarini^{ab,52} M. Carpinelli^{ab,52,††} G. Casarosa^{ab,52} M. Chrzaszcz^{a,52} F. Forti^{ab,52} M. A. Giorgi^{ab,52} A. Lusiani^{ac,52} B. Oberhof^{ab,52} E. Paoloni^{ab,52} G. Rizzo^{ab,52} J. J. Walsh^{a,52} D. Lopes Pegna,⁵³ J. Olsen,⁵³ A. J. S. Smith,⁵³ F. Anulli^{a,54} R. Faccini^{ab,54} F. Ferrarotto^{a,54} F. Ferroni^{ab,54} M. Gaspero^{ab,54} A. Pilloni^{ab,54} G. Piredda^{a,54} C. Büniger,⁵⁵ S. Dittrich,⁵⁵ O. Grünberg,⁵⁵ M. Hess,⁵⁵ T. Leddig,⁵⁵ C. Voß,⁵⁵ R. Waldi,⁵⁵ T. Adye,⁵⁶ E. O. Olaiya,⁵⁶ F. F. Wilson,⁵⁶ S. Emery,⁵⁷ G. Vasseur,⁵⁷ D. Aston,⁵⁸ D. J. Bard,⁵⁸ C. Cartaro,⁵⁸ M. R. Convery,⁵⁸ J. Dorfan,⁵⁸ G. P. Dubois-Felsmann,⁵⁸ W. Dunwoodie,⁵⁸ M. Ebert,⁵⁸ R. C. Field,⁵⁸ B. G. Fulsom,⁵⁸ M. T. Graham,⁵⁸ C. Hast,⁵⁸ W. R. Innes,⁵⁸ P. Kim,⁵⁸ D. W. G. S. Leith,⁵⁸ D. Lindemann,⁵⁸ S. Luitz,⁵⁸ V. Luth,⁵⁸ H. L. Lynch,⁵⁸ D. B. MacFarlane,⁵⁸ D. R. Muller,⁵⁸ H. Neal,⁵⁸ M. Perl,^{58,¶¶} T. Pulliam,⁵⁸ B. N. Ratcliff,⁵⁸ A. Roodman,⁵⁸ R. H. Schindler,⁵⁸ A. Snyder,⁵⁸ D. Su,⁵⁸ M. K. Sullivan,⁵⁸ J. Va'vra,⁵⁸ W. J. Wisniewski,⁵⁸ H. W. Wulsin,⁵⁸ M. V. Purohit,⁵⁹ J. R. Wilson,⁵⁹ A. Randle-Conde,⁶⁰ S. J. Sekula,⁶⁰ M. Bellis,⁶¹ P. R. Burchat,⁶¹ E. M. T. Puccio,⁶¹ M. S. Alam,⁶² J. A. Ernst,⁶² R. Gorodeisky,⁶³ N. Guttman,⁶³ D. R. Peimer,⁶³ A. Soffer,⁶³ S. M. Spanier,⁶⁴ J. L. Ritchie,⁶⁵ R. F. Schwitters,⁶⁵ J. M. Izen,⁶⁶ X. C. Lou,⁶⁶ F. Bianchi^{ab,67} F. De Mori^{ab,67} A. Filippi^{a,67} D. Gamba^{ab,67} L. Lanceri^{ab,68} L. Vitale^{ab,68} F. Martinez-Vidal,⁶⁹ A. Oyanguren,⁶⁹ P. Villanueva-Perez,⁶⁹ J. Albert,⁷⁰ Sw. Banerjee,⁷⁰ A. Beaulieu,⁷⁰ F. U. Bernlochner,⁷⁰ H. H. F. Choi,⁷⁰ G. J. King,⁷⁰ R. Kowalewski,⁷⁰ M. J. Lewczuk,⁷⁰ T. Lueck,⁷⁰ I. M. Nugent,⁷⁰ J. M. Roney,⁷⁰ R. J. Sobie,⁷⁰ N. Tasneem,⁷⁰ T. J. Gershon,⁷¹ P. F. Harrison,⁷¹ T. E. Latham,⁷¹ H. R. Band,⁷² S. Dasu,⁷² Y. Pan,⁷² R. Prepost,⁷² and S. L. Wu⁷²

(The BABAR Collaboration)

¹Laboratoire d'Annecy-le-Vieux de Physique des Particules (LAPP),
Université de Savoie, CNRS/IN2P3, F-74941 Annecy-Le-Vieux, France

²Universitat de Barcelona, Facultat de Física, Departament ECM, E-08028 Barcelona, Spain

³INFN Sezione di Bari^a; Dipartimento di Fisica, Università di Bari^b, I-70126 Bari, Italy

- ⁴University of Bergen, Institute of Physics, N-5007 Bergen, Norway
- ⁵Lawrence Berkeley National Laboratory and University of California, Berkeley, California 94720, USA
- ⁶Ruhr Universität Bochum, Institut für Experimentalphysik 1, D-44780 Bochum, Germany
- ⁷University of British Columbia, Vancouver, British Columbia, Canada V6T 1Z1
- ⁸Brunel University, Uxbridge, Middlesex UB8 3PH, United Kingdom
- ⁹Budker Institute of Nuclear Physics SB RAS, Novosibirsk 630090^a,
Novosibirsk State University, Novosibirsk 630090^b,
Novosibirsk State Technical University, Novosibirsk 630092^c, Russia
- ¹⁰University of California at Irvine, Irvine, California 92697, USA
- ¹¹University of California at Riverside, Riverside, California 92521, USA
- ¹²University of California at Santa Barbara, Santa Barbara, California 93106, USA
- ¹³University of California at Santa Cruz, Institute for Particle Physics, Santa Cruz, California 95064, USA
- ¹⁴California Institute of Technology, Pasadena, California 91125, USA
- ¹⁵University of Cincinnati, Cincinnati, Ohio 45221, USA
- ¹⁶University of Colorado, Boulder, Colorado 80309, USA
- ¹⁷Colorado State University, Fort Collins, Colorado 80523, USA
- ¹⁸Technische Universität Dortmund, Fakultät Physik, D-44221 Dortmund, Germany
- ¹⁹Laboratoire Leprince-Ringuet, Ecole Polytechnique, CNRS/IN2P3, F-91128 Palaiseau, France
- ²⁰University of Edinburgh, Edinburgh EH9 3JZ, United Kingdom
- ²¹INFN Sezione di Ferrara^a; Dipartimento di Fisica e Scienze della Terra, Università di Ferrara^b, I-44122 Ferrara, Italy
- ²²INFN Laboratori Nazionali di Frascati, I-00044 Frascati, Italy
- ²³INFN Sezione di Genova^a; Dipartimento di Fisica, Università di Genova^b, I-16146 Genova, Italy
- ²⁴Indian Institute of Technology Guwahati, Guwahati, Assam, 781 039, India
- ²⁵Universität Heidelberg, Physikalisches Institut, D-69120 Heidelberg, Germany
- ²⁶Humboldt-Universität zu Berlin, Institut für Physik, D-12489 Berlin, Germany
- ²⁷University of Iowa, Iowa City, Iowa 52242, USA
- ²⁸Iowa State University, Ames, Iowa 50011-3160, USA
- ²⁹Physics Department, Jazan University, Jazan 22822, Kingdom of Saudi Arabia
- ³⁰Johns Hopkins University, Baltimore, Maryland 21218, USA
- ³¹Laboratoire de l'Accélérateur Linéaire, IN2P3/CNRS et Université Paris-Sud 11,
Centre Scientifique d'Orsay, F-91898 Orsay Cedex, France
- ³²Lawrence Livermore National Laboratory, Livermore, California 94550, USA
- ³³University of Liverpool, Liverpool L69 7ZE, United Kingdom
- ³⁴Queen Mary, University of London, London, E1 4NS, United Kingdom
- ³⁵University of London, Royal Holloway and Bedford New College, Egham, Surrey TW20 0EX, United Kingdom
- ³⁶University of Louisville, Louisville, Kentucky 40292, USA
- ³⁷Johannes Gutenberg-Universität Mainz, Institut für Kernphysik, D-55099 Mainz, Germany
- ³⁸University of Manchester, Manchester M13 9PL, United Kingdom
- ³⁹University of Maryland, College Park, Maryland 20742, USA
- ⁴⁰Massachusetts Institute of Technology, Laboratory for Nuclear Science, Cambridge, Massachusetts 02139, USA
- ⁴¹McGill University, Montréal, Québec, Canada H3A 2T8
- ⁴²INFN Sezione di Milano^a; Dipartimento di Fisica, Università di Milano^b, I-20133 Milano, Italy
- ⁴³University of Mississippi, University, Mississippi 38677, USA
- ⁴⁴Université de Montréal, Physique des Particules, Montréal, Québec, Canada H3C 3J7
- ⁴⁵INFN Sezione di Napoli^a; Dipartimento di Scienze Fisiche,
Università di Napoli Federico II^b, I-80126 Napoli, Italy
- ⁴⁶NIKHEF, National Institute for Nuclear Physics and High Energy Physics, NL-1009 DB Amsterdam, The Netherlands
- ⁴⁷University of Notre Dame, Notre Dame, Indiana 46556, USA
- ⁴⁸Ohio State University, Columbus, Ohio 43210, USA
- ⁴⁹INFN Sezione di Padova^a; Dipartimento di Fisica, Università di Padova^b, I-35131 Padova, Italy
- ⁵⁰Laboratoire de Physique Nucléaire et de Hautes Energies,
IN2P3/CNRS, Université Pierre et Marie Curie-Paris6,
Université Denis Diderot-Paris7, F-75252 Paris, France
- ⁵¹INFN Sezione di Perugia^a; Dipartimento di Fisica, Università di Perugia^b, I-06123 Perugia, Italy
- ⁵²INFN Sezione di Pisa^a; Dipartimento di Fisica,
Università di Pisa^b; Scuola Normale Superiore di Pisa^c, I-56127 Pisa, Italy
- ⁵³Princeton University, Princeton, New Jersey 08544, USA
- ⁵⁴INFN Sezione di Roma^a; Dipartimento di Fisica,
Università di Roma La Sapienza^b, I-00185 Roma, Italy
- ⁵⁵Universität Rostock, D-18051 Rostock, Germany
- ⁵⁶Rutherford Appleton Laboratory, Chilton, Didcot, Oxon, OX11 0QX, United Kingdom
- ⁵⁷CEA, Irfu, SPP, Centre de Saclay, F-91191 Gif-sur-Yvette, France
- ⁵⁸SLAC National Accelerator Laboratory, Stanford, California 94309 USA
- ⁵⁹University of South Carolina, Columbia, South Carolina 29208, USA

⁶⁰*Southern Methodist University, Dallas, Texas 75275, USA*

⁶¹*Stanford University, Stanford, California 94305-4060, USA*

⁶²*State University of New York, Albany, New York 12222, USA*

⁶³*Tel Aviv University, School of Physics and Astronomy, Tel Aviv, 69978, Israel*

⁶⁴*University of Tennessee, Knoxville, Tennessee 37996, USA*

⁶⁵*University of Texas at Austin, Austin, Texas 78712, USA*

⁶⁶*University of Texas at Dallas, Richardson, Texas 75083, USA*

⁶⁷*INFN Sezione di Torino^a; Dipartimento di Fisica, Università di Torino^b, I-10125 Torino, Italy*

⁶⁸*INFN Sezione di Trieste^a; Dipartimento di Fisica, Università di Trieste^b, I-34127 Trieste, Italy*

⁶⁹*IFIC, Universitat de Valencia-CSIC, E-46071 Valencia, Spain*

⁷⁰*University of Victoria, Victoria, British Columbia, Canada V8W 3P6*

⁷¹*Department of Physics, University of Warwick, Coventry CV4 7AL, United Kingdom*

⁷²*University of Wisconsin, Madison, Wisconsin 53706, USA*

A search is presented for the decay $\Upsilon(1S) \rightarrow \gamma A^0$, $A^0 \rightarrow c\bar{c}$, where A^0 is a candidate for the CP -odd Higgs boson of the next-to-minimal supersymmetric standard model. The search is based on data collected with the *BABAR* detector at the $\Upsilon(2S)$ resonance. A sample of $\Upsilon(1S)$ mesons is selected via the decay $\Upsilon(2S) \rightarrow \pi^+\pi^-\Upsilon(1S)$. The $A^0 \rightarrow c\bar{c}$ decay is identified through the reconstruction of hadronic D^0 , D^+ , and $D^*(2010)^+$ meson decays. No significant signal is observed. The measured 90% confidence-level upper limits on the product branching fraction $\mathcal{B}(\Upsilon(1S) \rightarrow \gamma A^0) \times \mathcal{B}(A^0 \rightarrow c\bar{c})$ range from 7.4×10^{-5} to 2.4×10^{-3} for A^0 masses from 4.00 to 8.95 GeV/ c^2 and 9.10 to 9.25 GeV/ c^2 , where the region between 8.95 and 9.10 GeV/ c^2 is excluded because of background from $\Upsilon(2S) \rightarrow \gamma\chi_{bJ}(1P)$, $\chi_{bJ}(1P) \rightarrow \gamma\Upsilon(1S)$ decays.

PACS numbers: 12.15.Ji, 12.60.Fr, 13.20.Gd, 14.80.Da

The next-to-minimal supersymmetric standard model (NMSSM) is an appealing extension of the standard model (SM). It solves the μ -problem of the minimal supersymmetric standard model and the hierarchy problem of the SM [1, 2]. The NMSSM has a rich Higgs sector of two charged, three neutral CP -even, and two neutral CP -odd bosons. Although the Higgs boson discovered at the CERN LHC [3, 4] is consistent with the SM Higgs boson, it can also be interpreted as one of the heavier Higgs bosons of the NMSSM [5]. The least heavy of the NMSSM Higgs bosons, denoted A^0 , could be light enough to be produced in the decay of an Υ meson [1, 6].

In the context of type I or type II two-Higgs-doublet models, the branching fractions of the A^0 depend on the A^0 mass and the NMSSM parameter $\tan\beta$ [7]. Below the charm mass threshold, the A^0 preferentially decays into two gluons if $\tan\beta$ is of order 1, and to $s\bar{s}$ or to $\mu^+\mu^-$ if $\tan\beta$ is of order 10. Above the charm mass threshold, the A^0 decays mainly to $c\bar{c}$ for $\tan\beta$ of order 1 and to $\tau^+\tau^-$ for $\tan\beta$ of order 10. *BABAR* has already ruled out much of the NMSSM parameter space for A^0 masses below the charm mass threshold through searches

for $A^0 \rightarrow \mu^+\mu^-$ [8, 9] and for $A^0 \rightarrow gg$ or $s\bar{s}$ [10]. Above the charm mass threshold, *BABAR* has ruled out some of the parameter space for high $\tan\beta$ with the $A^0 \rightarrow \tau^+\tau^-$ searches [11, 12]. None of the searches from *BABAR* have observed a significant signal, nor have the searches in leptonic channels from the CMS and CLEO [13–15] Collaborations. The $A^0 \rightarrow c\bar{c}$ channel is one of the last channels that has not yet been explored.

We report a search for the decay $\Upsilon(1S) \rightarrow \gamma A^0$, $A^0 \rightarrow c\bar{c}$ with A^0 masses ranging between 4.00 and 9.25 GeV/ c^2 . An $\Upsilon(1S)$ decay is tagged by the presence of a pion pair from $\Upsilon(2S) \rightarrow \pi^+\pi^-\Upsilon(1S)$. An $A^0 \rightarrow c\bar{c}$ decay is tagged by the presence of at least one charmed meson such as a D^0 , a D^+ , or a $D^*(2010)^+$. Therefore candidates are constructed from the combination of a photon, a D meson, and a dipion candidate. An exclusive reconstruction of the A^0 is not attempted. Instead, a search is performed in the spectrum of the invariant mass of the system that recoils against the dipion-photon system. The analysis is therefore sensitive to the production of any charm resonance produced in the radiative decays of the $\Upsilon(1S)$ meson.

The data were recorded with the *BABAR* detector at the PEP-II asymmetric-energy e^+e^- collider at the SLAC National Accelerator Laboratory. The *BABAR* detector is described in detail elsewhere [16, 17]. We use 13.6 fb^{-1} of “on-resonance” data collected at the $\Upsilon(2S)$ resonance, corresponding to $(98.3 \pm 0.9) \times 10^6$ $\Upsilon(2S)$ mesons [18], which includes an estimated $(17.5 \pm 0.3) \times 10^6$ $\Upsilon(2S) \rightarrow \pi^+\pi^-\Upsilon(1S)$ decays [19]. The non- $\Upsilon(2S)$ backgrounds are studied using 1.4 fb^{-1} of “off-resonance” data collected 30 MeV below the $\Upsilon(2S)$ resonance.

The EvtGen event generator [20] is used to simulate the signal event decay chain, $e^+e^- \rightarrow \Upsilon(2S) \rightarrow$

*Now at: University of Tabuk, Tabuk 71491, Saudi Arabia

†Also at: Università di Perugia, Dipartimento di Fisica, I-06123 Perugia, Italy

‡Now at: Laboratoire de Physique Nucléaire et de Hautes Energies, IN2P3/CNRS, F-75252 Paris, France

§Now at: University of Huddersfield, Huddersfield HD1 3DH, UK

¶Deceased

**Now at: University of South Alabama, Mobile, Alabama 36688, USA

††Also at: Università di Sassari, I-07100 Sassari, Italy

$\pi^+\pi^-\Upsilon(1S), \Upsilon(1S) \rightarrow \gamma A^0, A^0 \rightarrow c\bar{c}$, for A^0 masses between 4.0 and 9.0 GeV/c^2 in 0.5 GeV/c^2 steps and for A^0 masses of 9.2, 9.3, and 9.4 GeV/c^2 . The A^0 decay width is assumed to be 1 MeV. The hadronization of the $c\bar{c}$ system is simulated using the Jetset [21] program. The detector response is simulated with the GEANT4 [22] suite of programs.

Photon candidates are required to have an energy greater than 30 MeV and a Zernike moment A_{42} [23] less than 0.1. The A_{42} selection reduces contributions from hadronic showers identified as photons. Events are required to contain at least one photon candidate. Each photon candidate is taken in turn to represent the radiative photon in the $\Upsilon(1S) \rightarrow \gamma A^0$ decays. We do not select a best signal candidate, neither for the radiative photon nor for the D meson and dipion candidates discussed below, but rather allow multiple candidates in an event.

Events must contain at least one D meson candidate, which is reconstructed in five channels: $D^0 \rightarrow K^-\pi^+$, $D^+ \rightarrow K^-\pi^+\pi^+$, $D^0 \rightarrow K^-\pi^+\pi^+\pi^-$, $D^0 \rightarrow K_s^0\pi^+\pi^-$, and $D^*(2010)^+ \rightarrow \pi^+D^0$ with $D^0 \rightarrow K^-\pi^+\pi^0$. The $D^0 \rightarrow K^-\pi^+\pi^0$ decays are reconstructed in the $D^*(2010)^+$ production channel to reduce a large background that would otherwise be present. The inclusion of charge conjugate processes is implied. The π^0 candidates are reconstructed from two photon candidates by requiring the invariant mass of the reconstructed π^0 to lie between 100 and 160 MeV/c^2 . The π^0 candidates do not make use of the radiative photon candidate. The K_s^0 candidates are reconstructed from two oppositely charged pion candidates. Each K_s^0 candidate must have a reconstructed mass within 25 MeV/c^2 of the nominal K_s^0 mass [19] and satisfy $d/\sigma_d > 3$, where d is the distance between the reconstructed e^+e^- collision point and the K_s^0 vertex, with σ_d the uncertainty of d .

The D^0 and D^+ candidates are required to have masses within 20 MeV/c^2 of their nominal masses [19], corresponding to 3 to 4 standard deviations (σ) in their mass resolution. When reconstructing $D^*(2010)^+$ candidates, we constrain the $D^0 \rightarrow K^-\pi^+\pi^0$ candidate mass to its nominal value [19]. The $D^*(2010)^+$ candidate mass distribution has longer tails. The $D^*(2010)^+$ candidates are required to lie within 5 MeV/c^2 of its nominal mass [19], corresponding to 10 σ in the mass resolution.

Events are required to have at least one dipion candidate, constructed from two oppositely charged tracks. The invariant mass, m_R , of the system recoiling against the dipion in the $\Upsilon(2S) \rightarrow \pi^+\pi^-\Upsilon(1S)$ transition is calculated by

$$m_R^2 = M_{\Upsilon(2S)}^2 + m_{\pi\pi}^2 - 2M_{\Upsilon(2S)}E_{\pi\pi}, \quad (1)$$

where $m_{\pi\pi}$ is the measured dipion mass, $M_{\Upsilon(2S)}$ is the nominal $\Upsilon(2S)$ mass [19], and $E_{\pi\pi}$ is the dipion energy in the e^+e^- center-of-mass (CM) frame. The two pions in the dipion system are required to arise from a common vertex. Signal candidates must satisfy $9.45 < m_R < 9.47$ GeV/c^2 . Figure 1 presents the distribution of m_R

after application of these criteria. A clear peak is seen at the $\Upsilon(1S)$ mass.

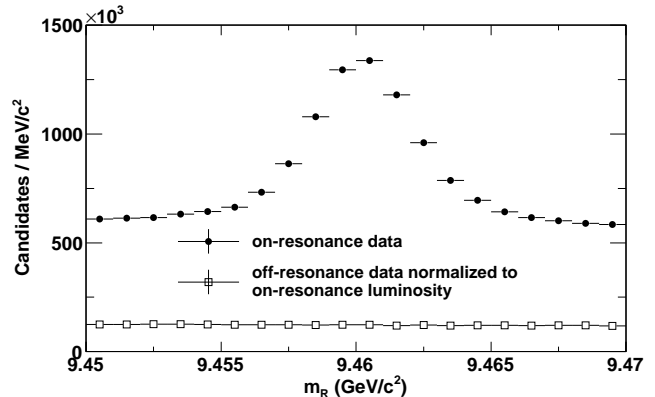


FIG. 1: The m_R distribution of events with a dipion, charm, and photon tag before application of selection criteria based on the BDT output (see text). The solid circles indicate the on-resonance data. The open squares indicate the off-resonance data normalized to the on-resonance luminosity.

All charged tracks and calorimeter clusters other than those used to define the radiative photon, the D meson candidate, and the dipion candidate are referred to as the “rest of the event”.

The mass of the A^0 candidate, m_X , is determined from the mass of the system recoiling against the dipion and photon through

$$m_X^2 = (P_{e^+e^-} - P_{\pi^+\pi^-} - P_\gamma)^2, \quad (2)$$

where P denotes four-momentum measured in the CM frame. The four-momentum of the e^+e^- system is given by $P_{e^+e^-} = (M_{\Upsilon(2S)}, 0, 0, 0)$.

Backgrounds are evaluated using simulated $\Upsilon(2S)$ and $e^+e^- \rightarrow q\bar{q}$ events, where q is a $u, d, s,$ or c quark. Events with low-energy photons contribute a large background for m_X greater than 7.50 GeV/c^2 . Therefore, the analysis is divided into a low A^0 mass region (4.00 to 8.00 GeV/c^2) and a high A^0 mass region (7.50 to 9.25 GeV/c^2). The definitions of the regions, which overlap, are motivated by the need to have sufficient statistical precision for the background determination in each region.

We train ten boosted decision tree (BDT) classifiers [24] to separate background from signal candidates (two mass regions \times five D channels). The BDTs are trained using samples of simulated signal events, simulated generic $\Upsilon(2S)$ events, and the off-resonance data. The BDT inputs consist of 24 variables:

1-2. Event variables:

- number of charged tracks in the event,
- number of calorimeter clusters in the event.

3-12. Kinematic variables:

- m_R ,

- dipion likelihood (defined later),
- D candidate mass,
- D candidate momentum,
- photon π^0 score (defined later),
- energy of the most energetic charged track in the rest of the event, calculated using a charged pion mass hypothesis,
- energy of the most energetic calorimeter cluster in the rest of the event,
- invariant mass of the rest of the event,
- CM frame momentum of the rest of the event,
- CM frame energy of the rest of the event.

13-15. Vertex variables:

- transverse coordinate of a vertex formed using all charged tracks,
- longitudinal coordinate of a vertex formed using all charged tracks,
- the χ^2 probability of a vertex fit using all charged tracks.

16-18. Event shape variables:

- the ratio of the second to zeroth Fox-Wolfram moment [25], calculated using all charged tracks and calorimeter clusters,
- sphericity [26] of the event,
- magnitude of the thrust [27].

19-24. Opening angles in the CM frame between the

- dipion and photon candidate,
- dipion and D candidate,
- dipion and thrust axis,
- photon and D candidate,
- photon and thrust axis,
- D candidate and thrust axis.

The kinematic variables provide the most separation power for all ten BDTs. The separation power of the other variables depends on the mass region and channel. The vertex variables suppress background without a D meson in the event. The event shape variables suppress $e^+e^- \rightarrow q\bar{q}$ backgrounds.

The dipion likelihood [24] is defined using the opening angle between the two charged pions in the CM frame, the transverse momentum of the pair, the invariant mass of the pair, the larger of the two momenta of the pair, and the χ^2 probability of the pair's vertex fit.

To reject photon candidates from $\pi^0 \rightarrow \gamma\gamma$ decays, a likelihood [24] is defined using the invariant mass of the radiative photon candidate and a second photon (if present), and the second photon's CM energy. The lower the likelihood, the more π^0 -like the photon pair. The

photon π^0 score is the minimum likelihood formed from the radiative photon and any other photon in the event excluding photon candidates used to reconstruct the π^0 candidate in the $D^0 \rightarrow K^- \pi^+ \pi^0$ decay.

For each channel and mass range, each BDT output variable is required to exceed a value determined by maximizing the quantity $S/(1.5 + \sqrt{B})$ [28], where S and B are the expected numbers of signal and background events, respectively, based on simulation.

In the case of events with multiple signal candidates that satisfy the selection criteria, there may be multiple values of m_X . Signal candidates that have the same dipion and radiative photon candidate have the same value of m_X , irrespective of which D candidate is used. We reject a signal candidate if its value of m_X has already been used.

In total, 9.8×10^3 and 7.4×10^6 candidates satisfy the selection criteria in the low- and high-mass regions, respectively. The corresponding distributions of m_X are shown in Fig. 2. The backgrounds in the low-mass region consist of $\Upsilon(1S) \rightarrow \gamma gg$ (35%); other $\Upsilon(1S)$ decays, denoted $\Upsilon(1S) \rightarrow X$ (34%); $\Upsilon(2S)$ decays without a dipion transition, denoted $\Upsilon(2S) \rightarrow X$ (15%); and $e^+e^- \rightarrow q\bar{q}$ events (16%). The corresponding background contributions in the high-mass region are 1%, 66%, 18%, and 15%. Background contributions from $\Upsilon(1S) \rightarrow \gamma gg$ decays reach a maximum near $5.5 \text{ GeV}/c^2$ and decrease above $7 \text{ GeV}/c^2$.

We search for the A^0 resonance as a peak in the m_X distribution. The reconstructed width of the A^0 is expected to strongly depend on its mass due to better photon energy resolution at lower photon energies. Therefore, an extended maximum likelihood fit in a local mass range is performed as a function of test-mass values, denoted m_{A^0} . For these fits, the parameters of the probability density function (PDF) used to model the shape of the signal distribution are fixed. The parameters of the background PDF, the number of signal events N_{sig} , and the number of background events are determined in the fit.

The signal m_X PDF is modeled with a Crystal Ball function [29], which consists of a Gaussian and a power-law component. The values of the signal PDF at a given value of m_{A^0} are determined through interpolation from fits of simulated signal events at neighboring masses. The background m_X PDF is modeled with a second-order polynomial.

The fits are performed to the m_X spectrum, for various choices of m_{A^0} , in steps of 10 and 2 MeV/c^2 for the low- and high-mass regions, respectively. The step sizes are at least 3 times smaller than the width of the signal m_X PDF. We use a local fitting range of $\pm 10 \sigma_{CB}$ around m_{A^0} , where σ_{CB} denotes the width of the Gaussian component of the Crystal Ball function. The σ_{CB} parameter varies between 120 and 8 MeV/c^2 for values of m_{A^0} between 4.00 and $9.25 \text{ GeV}/c^2$, as shown in Fig. 3. We do not perform a fit for $8.95 < m_{A^0} < 9.10 \text{ GeV}/c^2$ because of a large background from $\Upsilon(2S) \rightarrow \gamma\chi_{bJ}(1P)$,

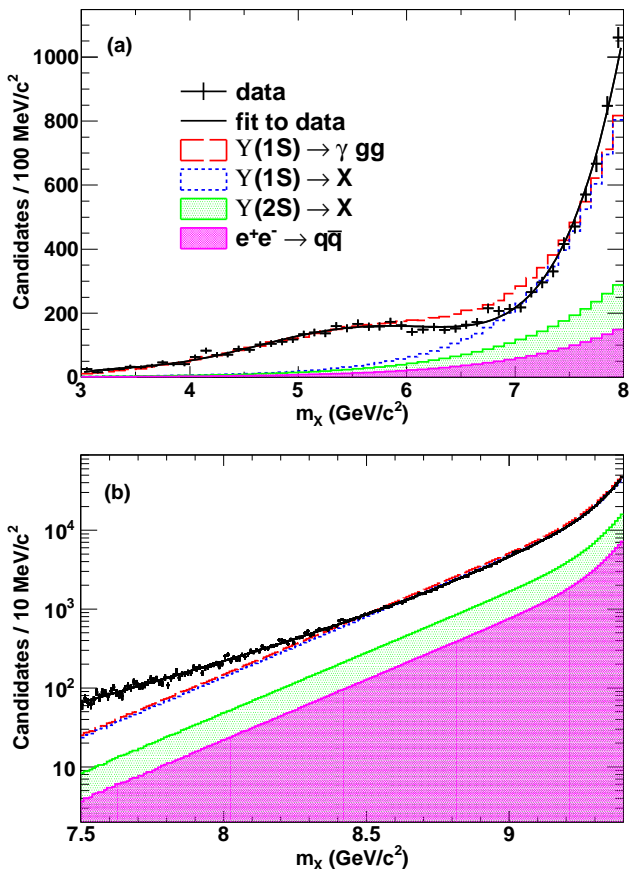


FIG. 2: The m_X distributions of signal candidates in the low- (a) and high- (b) mass regions after applying all selection criteria. The points indicate the data. The solid curve shows the result of a fit to the data under a background-only hypothesis. The colored histograms show the cumulative background contributions from $e^+e^- \rightarrow q\bar{q}$ (magenta dense-dot filled), $\Upsilon(2S) \rightarrow X$ (green sparse-dot filled), $\Upsilon(1S) \rightarrow X$ (blue dotted), and $\Upsilon(1S) \rightarrow \gamma gg$ (red dashed) events.

$\chi_{bJ}(1P) \rightarrow \gamma\Upsilon(1S)$ decays.

The fitting procedure is validated using background-only pseudo-experiments. The m_X PDF used to generate pseudo-experiments for the low-mass region is obtained from a fit of a fifth-order polynomial to the low-mass region data. The m_X PDF used for the high-mass region is obtained from a fit of the sum of four exponential functions plus six Crystal Ball functions to the high-mass region data, with shape parameters fixed according to expectations from simulation and with the relative normalizations determined in the fit. The Crystal Ball functions describe the $\Upsilon(2S) \rightarrow \gamma\chi_{bJ}(1P)$ and $\chi_{bJ}(1P) \rightarrow \gamma\Upsilon(1S)$ transitions while the exponential terms describe the non-resonant background. Four exponential terms are used because the non-resonant background increases rapidly for higher m_X . The background fits are overlaid in Fig. 2. The fitting procedure returns a null signal for most m_{A^0} values but is found to require a correction to N_{sig} for values of m_{A^0} near 4.00 or 9.25 GeV/c^2 . The correc-

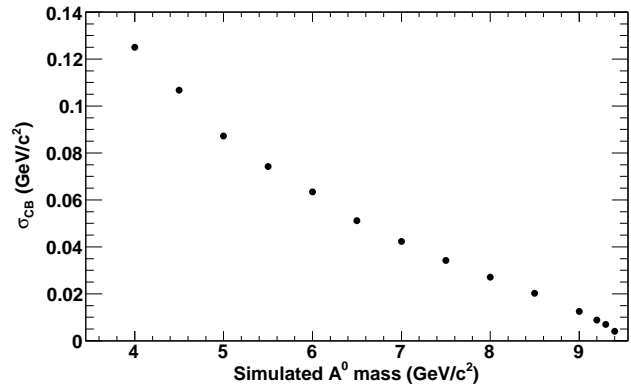


FIG. 3: The σ_{CB} parameter for A^0 decays of various simulated masses.

tions are determined from the average number of signal events found in the fits to the background-only pseudo-experiments. The corrections are applied as a function of m_{A^0} and reach a maximum of 15 and 50 candidates in the low- and high-mass regions, respectively. The uncertainty of the correction is assumed to be half its value.

The reconstruction efficiency takes into account the hadronization of the $c\bar{c}$ system into D mesons, the branching fraction of D mesons to the five decay channels, detector acceptance, and the BDT selection. The efficiencies range from 4.0% to 2.6% for simulated A^0 masses between 4.00 and 9.25 GeV/c^2 .

Potential bias introduced by the fitting procedure is evaluated using pseudo-experiments with different values of the product branching fraction $\mathcal{B}(\Upsilon(1S) \rightarrow \gamma A^0) \times \mathcal{B}(A^0 \rightarrow c\bar{c})$. For various choices of m_{A^0} , the extracted product branching fraction is found to be $(4 \pm 3)\%$ higher than the value used to generate the events. This result is used to define a correction and its uncertainty.

Table I summarizes all correction factors and associated systematic uncertainties. The fit correction systematic uncertainty is added in quadrature with the statistical uncertainty of N_{sig} . All other correction factors are added in quadrature and applied to the reconstruction efficiency. A correction of 1.00 means we do not apply any correction but propagate the multiplicative uncertainty.

The systematic uncertainties associated with the reconstruction efficiencies are dominated by the differences between data and simulation, including the BDT output modeling, $c\bar{c}$ hadronization, D -candidate mass resolution, dipion recoil mass and likelihood modeling, and photon reconstruction. Other systematic uncertainties are associated with the fit bias (discussed above), the dipion branching fraction [19], the finite size of the simulated signal sample, and the $\Upsilon(2S)$ counting [18].

The BDT output distributions in off-resonance data and $e^+e^- \rightarrow q\bar{q}$ simulation, shown in Fig. 4, have consistent shapes but are slightly shifted from one another. The associated systematic uncertainty is estimated by shifting the simulated distributions so that the mean val-

TABLE I: Summary of corrections and their associated systematic uncertainties. All corrections are multiplicative except for the fit correction.

Source	Low region	High region
Fit correction (candidates)	up to 15 ± 8	up to 50 ± 25
BDT output modeling	0.93 ± 0.04	0.98 ± 0.01
Source	Both regions	
$c\bar{c}$ hadronization	1.00 ± 0.09	
Fit bias	1.04 ± 0.03	
Dipion branching fraction	1.00 ± 0.02	
Photon reconstruction	0.967 ± 0.017	
D mass resolution	0.98 ± 0.01	
Finite simulation statistics	1.00 ± 0.01	
$\mathcal{Y}(2S)$ counting	1.00 ± 0.01	
Dipion likelihood	1.02 ± 0.01	
Dipion recoil mass	0.991 ± 0.005	

ues agree with the data, and then recalculating the efficiencies. The reconstruction efficiencies decrease by 7% and 2% in the low- and high-mass regions, respectively.

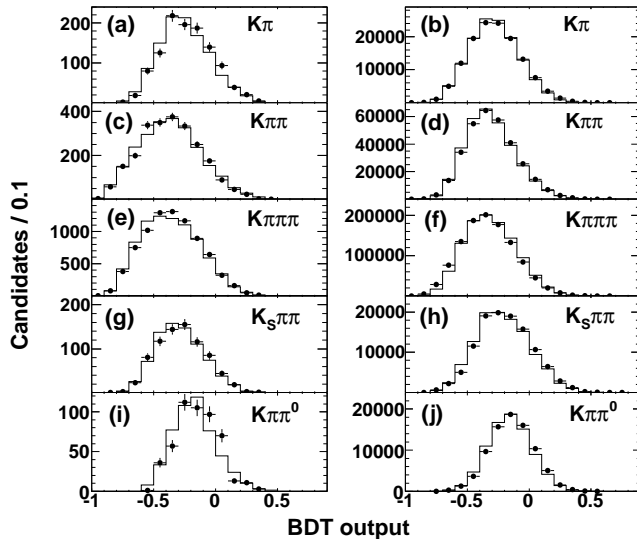


FIG. 4: The BDT distributions in off-resonance data (points) and simulated $e^+e^- \rightarrow q\bar{q}$ events (histograms) for the five D meson decay modes. The results on the left (a, c, e, g, i) and right (b, d, f, h, j) correspond to the low- and high-mass regions, respectively.

The uncertainty associated with $c\bar{c}$ hadronization is evaluated by comparing D meson production in off-resonance data and $e^+e^- \rightarrow c\bar{c}$ simulation normalized to the same luminosity. The difference in the yield varies from 1% to 9% for the five D decay channels. We conservatively assign a global multiplicative uncertainty of 9% that includes effects due to the hadronization modeling, particle identification, tracking, π^0 reconstruction, and luminosity determination of the off-resonance data.

The uncertainty due to the discrepancy between the reconstructed D mass resolution in data and simulation

is estimated by Gaussian smearing of the D mass input in simulation to match the data and measuring the difference in the reconstruction efficiency.

Further corrections to account for data and simulation differences in reconstruction efficiencies are estimated with similar methods. Corrections are applied to account for the dipion recoil mass reconstruction, the dipion likelihood modeling, and the photon reconstruction [30].

The highest observed local significance in the low-mass region is 2.3 standard deviations, including statistical uncertainties only, at $4.145 \text{ GeV}/c^2$. The corresponding result for the high-mass region is 2.0 standard deviations at $8.411 \text{ GeV}/c^2$. The fits are shown in Fig. 5. Such fluctuations occur in 54% and 80% of pseudo-experiments, respectively. Hence our data are consistent with the background-only hypothesis.

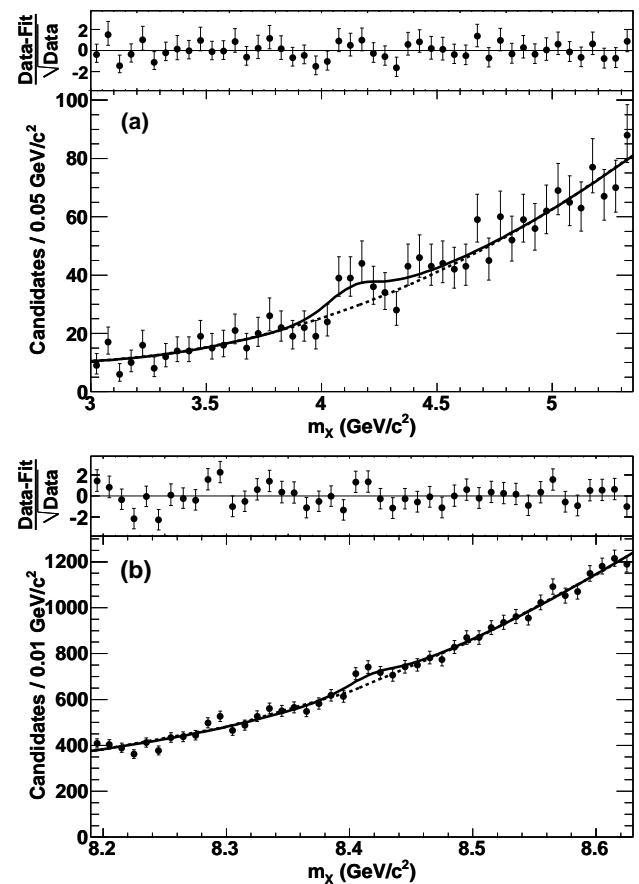


FIG. 5: The fits with the highest local significance in the low- (a) and high- (b) mass regions. The solid line is the fit that includes a signal. The dotted line is the background component of the solid line.

Upper limits on the product branching fraction $\mathcal{B}(\mathcal{Y}(1S) \rightarrow \gamma A^0) \times \mathcal{B}(A^0 \rightarrow c\bar{c})$ at 90% confidence level (C.L.) are determined assuming a uniform prior, with the constraint that the product branching fraction be greater than zero. The distribution of the likelihood function for N_{sig} is assumed to be Gaussian with a width equal to

the total uncertainty in N_{sig} . The upper limits obtained from the low-mass region are combined with those from the high-mass region to define a continuous spectrum for the upper limits. The results are shown in Fig. 6.

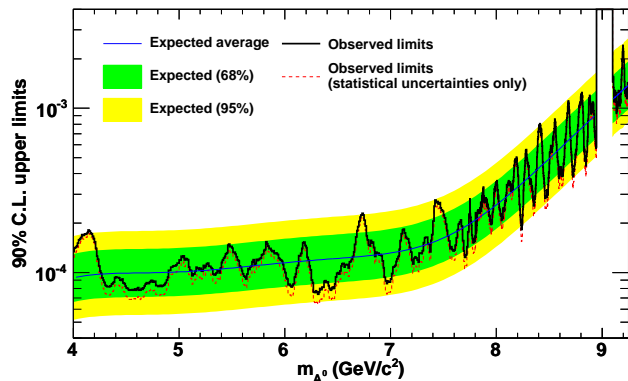


FIG. 6: (color online) The 90% C.L. upper limits on the product branching fraction $\mathcal{B}(\Upsilon(1S) \rightarrow \gamma A^0) \times \mathcal{B}(A^0 \rightarrow c\bar{c})$ using all uncertainties (thick line) and using statistical uncertainties only (thin dashed line). The inner and outer bands contain 68% and 95% of our expected upper limits. The bands are calculated using all uncertainties. The thin solid line in the center of the inner band is the expected upper limit.

In summary, we search for a resonance in radiative decays of the $\Upsilon(1S)$ with a charm tag. We do not observe a significant signal and set upper limits on the product branching fraction $\mathcal{B}(\Upsilon(1S) \rightarrow \gamma A^0) \times \mathcal{B}(A^0 \rightarrow c\bar{c})$ rang-

ing from 7.4×10^{-5} to 2.4×10^{-3} for A^0 masses from 4.00 to 9.25 GeV/c^2 , excluding masses from 8.95 to 9.10 GeV/c^2 because of background from $\Upsilon(2S) \rightarrow \gamma \chi_{bJ}(1P)$, $\chi_{bJ}(1P) \rightarrow \gamma \Upsilon(1S)$ decays. These results will further constrain the NMSSM parameter space.

We are grateful for the extraordinary contributions of our PEP-II colleagues in achieving the excellent luminosity and machine conditions that have made this work possible. The success of this project also relies critically on the expertise and dedication of the computing organizations that support BABAR. The collaborating institutions wish to thank SLAC for its support and the kind hospitality extended to them. This work is supported by the US Department of Energy and National Science Foundation, the Natural Sciences and Engineering Research Council (Canada), the Commissariat à l’Energie Atomique and Institut National de Physique Nucléaire et de Physique des Particules (France), the Bundesministerium für Bildung und Forschung and Deutsche Forschungsgemeinschaft (Germany), the Istituto Nazionale di Fisica Nucleare (Italy), the Foundation for Fundamental Research on Matter (The Netherlands), the Research Council of Norway, the Ministry of Education and Science of the Russian Federation, Ministerio de Economía y Competitividad (Spain), the Science and Technology Facilities Council (United Kingdom), and the Binational Science Foundation (U.S.-Israel). Individuals have received support from the Marie-Curie IEF program (European Union) and the A. P. Sloan Foundation (USA).

-
- [1] R. Dermisek, J. F. Gunion, and B. McElrath, Phys. Rev. D **76**, 051105(R) (2007).
 - [2] M. Maniatis, Int. J. Mod. Phys. A **25**, 3505 (2010).
 - [3] G. Aad *et al.* (ATLAS Collaboration), Phys. Lett. B **716** 1 (2012).
 - [4] S. Chatrchyan *et al.* (CMS Collaboration), Phys. Lett. B **716** 30 (2012).
 - [5] N. D. Christensen, T. Han, Z. Liu, and S. Su, J. High Energy Phys. **08** (2013) 019.
 - [6] F. Wilczek, Phys. Rev. Lett. **39**, 1304 (1977).
 - [7] R. Dermisek and J. F. Gunion, Phys. Rev. D **81**, 075003 (2010).
 - [8] B. Aubert *et al.* (BABAR Collaboration), Phys. Rev. Lett. **103**, 081803 (2009).
 - [9] J.P. Lees *et al.* (BABAR Collaboration), Phys. Rev. D **87**, 031102(R) (2013).
 - [10] J.P. Lees *et al.* (BABAR Collaboration), Phys. Rev. D **88**, 031701(R) (2013).
 - [11] B. Aubert *et al.* (BABAR Collaboration), Phys. Rev. Lett. **103**, 181801 (2009).
 - [12] J.P. Lees *et al.* (BABAR Collaboration), Phys. Rev. D **88**, 071102(R) (2013).
 - [13] S. Chatrchyan *et al.* (CMS Collaboration), Phys. Rev. Lett. **109**, 121801 (2012).
 - [14] S. Chatrchyan *et al.* (CMS Collaboration), Phys. Lett. B **726**, 564 (2013).
 - [15] W. Love *et al.* (CLEO Collaboration), Phys. Rev. Lett. **101**, 151802 (2008).
 - [16] B. Aubert *et al.* (BABAR Collaboration), Nucl. Instr. Methods Phys. Res. Sect. A **479**, 1 (2002).
 - [17] B. Aubert *et al.* (BABAR Collaboration), Nucl. Instr. Methods Phys. Res. Sect. A **729**, 615 (2013).
 - [18] J. P. Lees *et al.* (BABAR Collaboration), Nucl. Instr. Methods Phys. Res. Sect. A **726**, 203 (2013).
 - [19] K.A. Olive *et al.* (Particle Data Group), Chin. Phys. C **38**, 090001 (2014).
 - [20] D. J. Lange, Nucl. Instr. Methods Phys. Res. Sect. A **462**, 152 (2001).
 - [21] T. Sjöstrand, Comp. Phys. Comm. **82**, 74 (1994).
 - [22] S. Agostinelli *et al.* (GEANT4 Collaboration), Nucl. Instr. Methods Phys. Res. Sect. A **506**, 250 (2003).
 - [23] R. Sinkus and T.Voss, Nucl. Instr. Methods Phys. Res. Sect. A **391**, 360 (1997).
 - [24] A. Höcker *et al.*, PoS ACAT, 040 (2007), physics/0703039.
 - [25] G. C. Fox and S. Wolfram, Nucl. Phys. B **149**, 413 (1979).
 - [26] J. Bjorken and S. Brodsky, Phys. Rev. D **1**, 1416 (1970).
 - [27] S. Brandt *et al.*, Phys. Lett. **12**, 57 (1964).
 - [28] G. Punzi, preprint physics/0308063 (2003).
 - [29] M. J. Oreglia, Ph.D. Thesis, report SLAC-R-236 (1980), Appendix D.
 - [30] P. del Amo Sanchez *et al.* (BABAR Collaboration), Phys.

Rev. Lett. **107**, 021804 (2011).